

# Comparing four hard-sphere approximations for the low-temperature WCA melting line

Eman Attia, Jeppe C. Dyre, and Ulf R. Pedersen\*

*Glass and Time, IMFUFA, Department of Science and Environment,  
Roskilde University, P. O. Box 260, DK-4000 Roskilde, Denmark*

(Dated: May 3, 2022)

By combining interface-pinning simulations with numerical integration of the Clausius-Clapeyron equation we determine accurately the melting-line coexistence pressure and fluid/crystal densities of the Weeks-Chandler-Andersen (WCA) system covering four decades of temperature. The data are used for comparing the melting-line predictions of the Boltzmann, Andersen-Weeks-Chandler, Barker-Henderson, and Stillinger hard-sphere approximations. The Andersen-Weeks-Chandler and the Barker-Henderson theories give the most accurate predictions, and they both work excellently in the zero-temperature limit for which analytical expressions are derived here.

## I. INTRODUCTION

While systems of purely repulsive particles are rarely found in nature, they provide convenient models for both fluids and solids [1]. Examples are the inverse-power law (IPL) systems based on a homogeneous pair potential that varies with distance  $r$  as  $(r/\sigma)^{-n}$  in which  $\sigma$  is a length [2–5] and the exponential repulsive (EXP) pair potential that varies with distance as  $\exp(-r/\sigma)$  [6–8]. The oldest and most important purely repulsive system is that of hard spheres (HS) [9–12], which despite its simplicity provides a good zeroth-order model of realistic systems with both repulsive and attractive interactions [13–18]. A purely repulsive system has a single fluid phase and no gas-liquid phase transition. In contrast, the symmetry-breaking liquid-solid transition is present in all purely repulsive systems and, because of the absence of a gas phase, here the liquid-solid phase boundary extends to zero temperature.

This paper studies the noted Weeks, Chandler, and Andersen (WCA) purely repulsive system [17–44], which is arrived at by cutting and shifting the Lennard-Jones (LJ) interaction at its minimum [17]. In contrast to the IPL and EXP systems, the WCA pair potential has a finite range beyond which pair forces are zero, like those of the HS system. At the cutoff, the WCA pair potential and pair forces are smooth, and at low temperatures one expects HS approximations to apply because only insignificant “overlaps” are possible. Thus studies of the low-temperature melting line of the WCA system provides an excellent testing ground for comparing different HS approximations. This motivates the present study. In Sec. II we introduce the WCA system and the four HS approximations considered, as well as give a few simulation details. Section III details how we determined the WCA melting line by interface pinning and Clausius-Clapeyron integration. The predictions of the different HS approximations in regard to pressure and fluid/solid densities at melting are compared in Sec. IV. Finally,

Sec. V provides a brief outlook.

## II. THE WCA SYSTEM AND HARD-SPHERE APPROXIMATIONS

### A. The WCA system

We consider mono-disperse systems. Let  $\mathbf{R} = (\mathbf{r}_1, \mathbf{r}_2, \dots, \mathbf{r}_N)$  be the collective coordinate vector of  $N$  particles with mass  $m$  confined to the volume  $V$  (with periodic boundaries) and define the number density by  $\rho \equiv N/V$ . The potential part  $\mathcal{U}(\mathbf{R})$  of the Hamiltonian,  $\mathcal{H}(\mathbf{R}) = \mathcal{U}(\mathbf{R}) + \mathcal{K}(\dot{\mathbf{R}})$ , is assumed to be a sum of pair-potential contributions,

$$\mathcal{U}(\mathbf{R}) = \sum_{n>m}^N v(|\mathbf{r}_m - \mathbf{r}_n|). \quad (1)$$

We recall that the LJ pair potential is defined [45, 46] by

$$v(r) \equiv 4\varepsilon [(r/\sigma)^{-12} - (r/\sigma)^{-6}] \quad (2)$$

in which  $\varepsilon$  has units of energy and  $\sigma$  units of length. The WCA pair potential (Fig. 1) is defined by cutting and shifting the LJ potential at its minimum, which leads to [17]

$$v(r) = 4\varepsilon [(r/\sigma)^{-12} - (r/\sigma)^{-6}] + 1/4 \text{ for } r \leq r_c \quad (3)$$

and zero otherwise where

$$r_c = \sqrt[6]{2}\sigma \simeq 1.1225\sigma \quad (4)$$

The WCA pair potential is purely repulsive since the pair force  $-dv/dr \geq 0$  for all  $r$ 's, and it is smooth since both  $v(r)$  and its first derivative are continuous (the second derivative is discontinuous at  $r_c$ , though). All quantities obtained by simulations are below reported in units derived from  $m$ ,  $\sigma$ ,  $\varepsilon$  and the Boltzmann constant  $k_B$ .

Simulations of the WCA system are conducted using the RUMD software package version 3.5 [47]. An initial configuration is first constructed by replicating  $8 \times 8 \times$

\* ulf@urp.dk

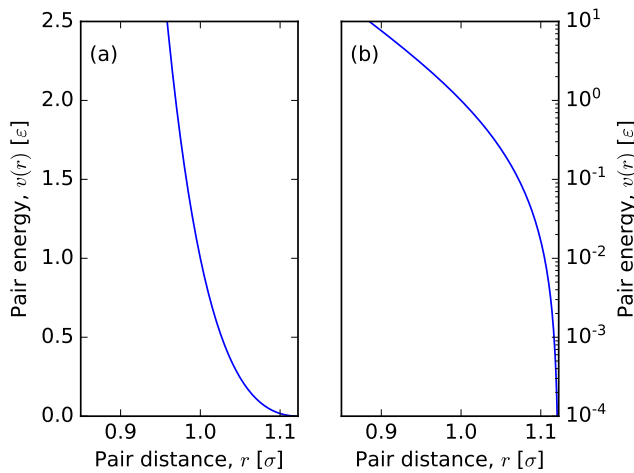


FIG. 1. (a) The WCA pair potential Eq. (3). (b) The same pair potential on a logarithmic energy scale, showing a steep slope at low pair energies.

20 face centered cubic (FCC) unit cells, resulting in a system of  $N = 5120$  particles. This initial configuration is then scaled uniformly to the desired density  $\rho$ . If a liquid configuration is needed, the crystal is melted in a high-temperature simulation. The Newtonian equations of motion are discretized using the leap-frog algorithm [48] with the temperature-dependent time step

$$dt = 0.001 \frac{\sigma}{\sqrt{k_B T/m}}. \quad (5)$$

Simulations in the  $NVT$  ensemble [47–51] are realized using a Langevin thermostat with relaxation time  $t_T = m/\alpha$  where  $\alpha$  is a friction coefficient given by

$$t_T = 0.2 \frac{\sigma}{\sqrt{k_B T/m}}. \quad (6)$$

For  $Np_z T$  Langevin simulations [47, 50, 51] we used the same thermostat relaxation time and the barostat relaxation time

$$t_p = 100 \frac{\sigma}{\sqrt{k_B T/m}}. \quad (7)$$

We have found that introducing this  $1/\sqrt{T}$  scaling to the relaxation times [52] provides a simple way to ensure stability and efficiency of computations spanning several orders of magnitude in temperature (see Ref. 43 for a different approach). Note that in this way the average number of steps needed to travel the distance  $\sigma$  for a thermal particle is the same for all temperatures.

## B. Hard-Sphere approximations to the WCA system

Perturbation theories have proven successful for describing many fluids near freezing [1, 15–25, 53–67]. The

basic assumption is that the pair interaction can be written as

$$v(r) = v_0(r) + v_1(r) \quad (8)$$

in which  $v_0(r)$  is the pair potential of a (well-known) reference system and  $v_1(r)$  is a small perturbation potential. Often, the HS system is used as the reference. Several suggestions have been made for choosing the appropriate HS diameter,  $d$ . Below we list four well-known HS criteria; in Sec. IV these are evaluated with respect to their ability to locate the solid-liquid coexistence line.

In the zero-temperature limit ( $T \rightarrow 0$ ) the WCA pair potential approaches that of a HS [9–12] system with diameter  $d = r_c$ , i.e., the system described by

$$v_d(r) = \infty \text{ for } r < d \quad (9)$$

and zero otherwise. While this may not be intuitively obvious since the WCA pair potential goes smoothly to zero at the cutoff, it becomes clear when the WCA potential is shown in a log-plot (Fig. 1(b)). The simplest way of assigning an effective HS diameter to a WCA particle is to use the truncation distance

$$d = r_c. \quad (10)$$

This criterion is exact for  $T \rightarrow 0$ . At finite temperatures, however, the effective HS diameter will be smaller, and here one needs to make some physical assumption in order to improve Eq. (10) to arrive at better approximations. We list below four such approximations.

### 1. Boltzmann's hard-sphere criterion

In his 1890 *Lectures on Gas Theory* [68] Boltzmann suggested that the effective HS diameter  $d$  should be identified with the distance of closest approach when the velocities of two head-on colliding particles are given by their average kinetic energy at far distances. This criterion can be written as

$$v(d) = k_B T, \quad (11)$$

which for the WCA system results in

$$d = \frac{r_c}{\sqrt[6]{1 + \sqrt{k_B T/\varepsilon}}}. \quad (12)$$

Boltzmann's idea, which provides the simplest HS approximation, has been used to estimate the effective HS diameter of the WCA system by a number of authors [19–22, 24, 25].

### 2. The Andersen-Weeks-Chandler hard-sphere criterion

A more sophisticated HS criterion was suggested in 1971 by Andersen, Weeks, and Chandler (AWC) [57].

Their motivation was to match as well as possible the Helmholtz free energy of the pair potential in question to the associated HS system. The AWC criterion may be summarized as follows. If

$$e(r) = \exp(-v(r)/k_B T) \quad (13)$$

is the pair-potential Boltzmann probability factor, the AWC effective HS diameter  $d$  is identified from

$$\int_0^\infty r^2 y_d(r) \Delta e(r) dr = 0 \quad (14)$$

in which  $\Delta e(r) = e(r) - e_d(r)$  is the blip function and  $y_d(r)$  the cavity function of the HS fluid. In the Percus-Yevic approximation the cavity function is given analytically [1, 60–63, 69, 70], which is convenient for applications of Eq. (14). The appearance of the blip function in Eq. (14) effectively limits the AWC integral to values near  $d$ . Thus it is sufficient to consider the zeroth and first shell of  $y_d(r)$  to evaluate the AWC integral of Eq. (14) with a high accuracy. We used the following implementation of the cavity function in the determination of the HS diameter  $d$  via Eq. (14) [61]. If  $s \equiv r/d$ ,

$$y_d(s) = \begin{cases} c_0 - c_1 s + c_3 s^3 & \text{for } s < 1 \\ H_1(s)/s & \text{for } 1 < s < 2 \end{cases} \quad (15)$$

where

$$\begin{aligned} H_1(s) = & a_1 \exp A(s-1)r \\ & + a_2 \exp B(s-1) \cos C(s-1) \\ & + a_3 \exp B(s-1) \sin C(s-1). \end{aligned} \quad (16)$$

The parameters depend on the packing fraction  $\eta$  (see Eqs. (6) and (15)–(17) in Ref. 61). For the coexistence packing fraction  $\eta = 0.4909$ , corresponding to the density  $\rho_l = 0.9375\sigma^{-3}$ , we have  $c_0 = 58.4514$ ,  $c_1 = 67.9928$ ,  $c_3 = 14.3461$ ,  $A = 1.58498$ ,  $B = -3.68494$ ,  $C = 3.85160$ ,  $a_1 = 0.56770$ ,  $a_2 = 4.23705$  and  $a_3 = -1.41141$ . We evaluated the AWC integral numerically using the Python module SciPy's [71] implementation of QUADPACK [72].

### 3. The Barker- Henderson hard-sphere criterion

The Barker and Henderson (BH) theory [56], which predates the AWC theory, can be viewed as a simplification of the AWC theory [1]. Specifically, it is assumed that  $r$ -squared times the cavity-function is a constant,  $r^2 y_d = \text{const.}$ , implying that Eq. (14) can be written

$$0 = \int_0^\infty [1 - e(r)] - [1 - e_d(r)] dr. \quad (17)$$

Since the integral of  $1 - e_d(r)$  is  $d$ , one arrives at the following HS criterion

$$d = \int_0^\infty [1 - e(r)] dr. \quad (18)$$

The  $r^2 y_d = \text{const.}$  assumption is reasonable since the blip function limits the integral to values near  $d$  where  $y_d$  does not change much when the temperature is sufficiently low. As  $T$  is lowered, the blip function narrows; thus the AWC diameter reduces to the BH criterion when  $T \rightarrow 0$ . Note that the BH criteria depends on temperature but not on density (the AWC criteria depends on both temperature and density). The BH integral of Eq. (18) is easily evaluated numerically using, e.g., the Python module SciPy's [71] implementation of QUADPACK [72].

### 4. Stillinger's hard-sphere criterion

At low temperatures, the integrand of the BH criterion Eq. (18) changes rapidly from nearly unity for  $r < d$  to nearly zero for  $r > d$ . This motivates the HS criterion proposed by Stillinger in 1976 [40, 73, 74]. He pragmatically identified the HS diameter from where the pair-potential Boltzmann factor equals one half, i.e.,

$$e(d) = \frac{1}{2}. \quad (19)$$

Stillinger introduced this in connection with his study of the Gaussian-core model [73]. The same idea can also be applied to the WCA potential, however, leading [40] to

$$d = \frac{r_c}{\sqrt[6]{1 + \sqrt{k_B T \ln(2)/\varepsilon}}}. \quad (20)$$

The functional form of this HS criterion is identical to that of Boltzmann if  $T$  is replaced by  $T \ln(2)$ : The factor 2 is here from Eq. (19), and with  $e(d) = 1/\exp(1)$  one arrives at Boltzmann's criterion [24].

## III. NUMERICAL DETERMINATION OF THE PHASE TRANSITION LINE

The interface pinning method [75–84] is used to compute the solid-liquid chemical potential difference  $\Delta\mu$  for isothermal state-points at temperatures  $0.002\varepsilon/k_B$ ,  $0.02\varepsilon/k_B$ ,  $0.2\varepsilon/k_B$ , and  $2\varepsilon/k_B$ . For a given temperature, we first set up a FCC crystal elongated in the  $z$ -direction with the given density and compute the equilibrium pressure in an  $NVT$  simulation. We then construct a configuration of half-crystal and half-fluid by a high-temperature simulation, where particle positions are only updated for half of the particles (resulting in melting for these particles). This produces a configuration similar to the one shown in the inset of Fig. 2. We then perform an  $Np_z T$  simulation by adding a harmonic bias-field to the potential part of the Hamiltonian,

$$\mathcal{U}_{\text{IP}}(\mathbf{R}) = \mathcal{U}(\mathbf{R}) + \frac{\kappa}{2} (Q(\mathbf{R}) - a)^2, \quad (21)$$

which forces the system toward configurations with a fluid-crystal interface. Here,  $\kappa$  and  $a$  are parameters of

TABLE I. Selected state points on the coexistence line determined with the interface pinning (IP) method and by numerical integration of the Clausius-Clapeyron (CC) relation (the Supplementary Material gives all computed data). The numbers in parenthesis give the statistical uncertainty (95% confidence interval).

$T [\varepsilon/k]$	$p [\varepsilon/\sigma^3]$	$\rho_l [1/\sigma^3]$	$\rho_s [1/\sigma^3]$	Method
20	633.309	1.78328	1.85850	CC
2	31.8086(66)	1.08441(5)	1.15192(6)	IP
2	31.7532	1.08413	1.15163	CC
0.2	2.05169(33)	0.80004(3)	0.87356(4)	IP
0.2	2.05118	0.79992	0.87358	CC
0.02	0.174944(47)	0.70638(5)	0.77889(6)	IP
0.002	0.016687(3)	0.67717(3)	0.74791(3)	IP
0.002	0.016680	0.67705	0.74792	CC

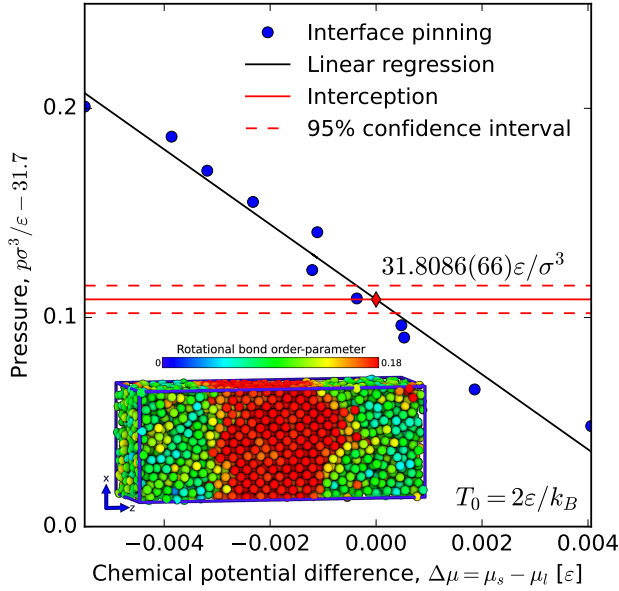


FIG. 2. Determination of the coexistence pressure at the temperature  $T_0 = 2\varepsilon/k_B$  (red diamond) by means of the interface-pinning method [75–84]. See the text for details. The inset shows an interface-pinned configuration where the colors indicate the rotational bond order parameter  $\bar{q}_4$  defined in Ref. 85. With this coloring crystalline particles are reddish, while fluid particles are greenish.

the bias-field, and  $Q(\mathbf{R})$  is an order-parameter that measure crystallinity through long-range order (see Eq. (15) in Ref. 75). The chemical potential difference between the two phases,  $\Delta\mu$ , is computed from the average force,  $\kappa(\langle Q(\mathbf{R}) \rangle - a)$ , which the bias field results in on the system (see Eq. (9) in Ref. 75). This is then repeated for several FCC densities (and thus pressures) near coexistence. As an example, Fig. 2 shows the pressures versus the computed chemical potentials at  $2\varepsilon/k_B$ , considering eleven pressures slightly above  $31.7\varepsilon/\sigma^3$ . The coexistence state point at  $\Delta\mu = 0$  is determined by linear regression, compare the solid line on Fig. 2. From this we find the coexistence pressure  $p = 31.8086(66)\varepsilon/\sigma^3$  where the

number in parenthesis gives the statistical error on the last two digits using a 95% confidence interval. Table I reports the thermodynamic coexistence data obtained by the interface-pinning (IP) method and numerical integration of the Clausius-Clapeyron (CC) relation as detailed below.

While the interface-pinning method is accurate and provides specific error estimates, it can be computationally expensive because long simulations are needed to properly represent interface fluctuations, which are usually significantly slower than fluctuations of the bulk solid and fluid [75]. As an alternative, we determine most points on the coexistence line by numerical integration of the Clausius-Clapeyron relation (below  $s$  and  $v$  are the entropy and volume per particle)

$$\frac{dp}{dT} = \frac{\Delta s}{\Delta v}. \quad (22)$$

This is an example of the Gibbs-Duhem integration methods discussed by Kofke [86, 87], which do not involve slow fluctuations of an interface. The volume difference  $\Delta v = v_l - v_s$  and the entropy difference  $\Delta s = s_l - s_s = (\Delta u + p\Delta v - \Delta\mu)/T$  can both be evaluated from standard  $NpT$  simulations of the two bulk phases at coexistence (where of course  $\Delta\mu = 0$ ).

We use a trapezoidal predictor-corrector method to compute coexistence pressures at the temperatures  $T_i = 0.02 \times 10^{(i/24)}$  where  $i$  is an integer, compare the solid black line on Fig. 3. Substituting  $t = T$  and  $y = p$  we can write the first-order differential equation to be solved in the standard form

$$y' = f(t, y) \quad (23)$$

where  $f$  is the slope evaluated as  $\Delta s/\Delta v$  (Eq.(22)). Suppose one knows the point  $(t_i, y_i)$  on the coexistence line, either from the interface-pinning method or from a previous step of the Clausius-Clapeyron integration, and wish to compute the next point  $(t_{i+1}, y_{i+1})$ . Let the step length in  $t$  be  $h = t_{i+1} - t_i$ . The prediction of the simple Euler algorithm is

$$y_{i+1}^{(0)} = y_i + hf(t_i, y_i). \quad (24)$$

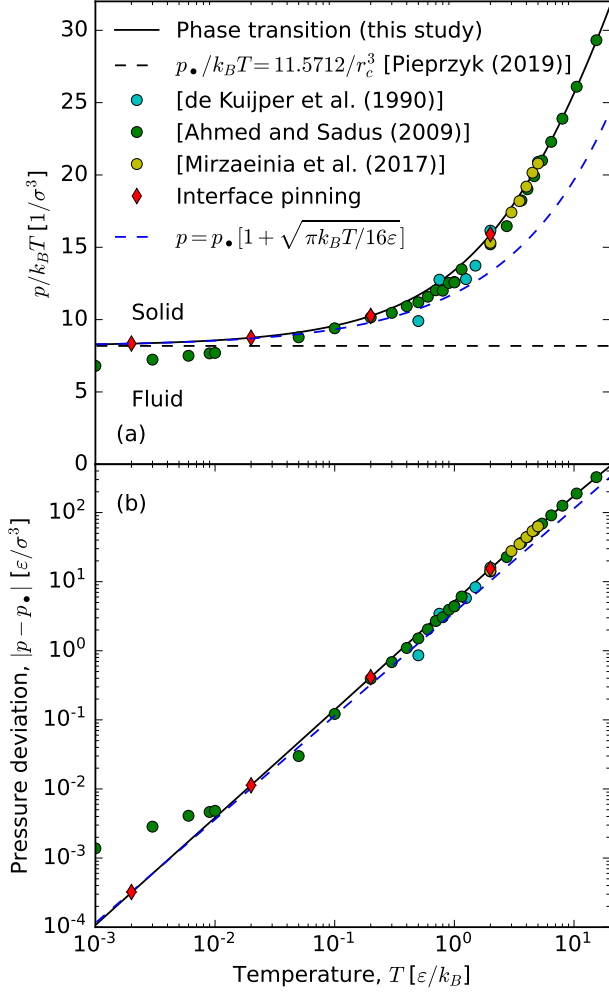


FIG. 3. Coexistence pressure as a function of the temperature. (a) The solid black line shows the reduced coexistence pressure  $p/k_B T$  as a function of the temperature (this study). The black dashed line gives the  $T \rightarrow 0$  HS limit,  $p_*/k_B T$ , and the colored dots represent literature coexistence pressures [42–44]. The red diamonds were computed with the interface-pinning method (this study). The blue dashed line shows that at low temperatures the pressure scales as  $T^{3/2}$ , as expected from HS theories (see the text). (b) The absolute value of the coexistence pressure in excess of its  $T \rightarrow 0$  limit.

A better estimate is provided using Heun’s method:

$$y_{i+1}^{(1)} = y_i + \frac{h}{2} [f(t_i, y_i) + f(t_i + h, y_{i+1}^0)] \quad (25)$$

The next estimate in an iterative predictor-corrector approach is

$$y_{i+1}^{(2)} = y_i + \frac{h}{2} [f(t_i, y_i) + f(t_i + h, y_{i+1}^1)] \quad (26)$$

or, in general,

$$y_{i+1}^{k+1} = y_i + \frac{h}{2} [f(t_i, y_i) + f(t_i + h, y_{i+1}^k)]. \quad (27)$$

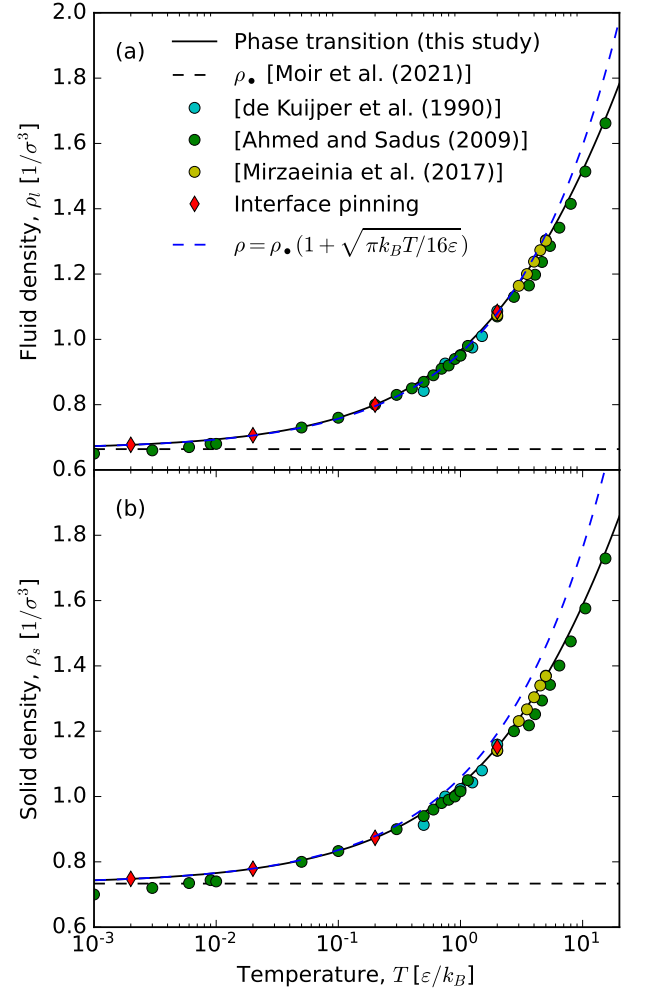


FIG. 4. Fluid density at freezing and solid density at melting as functions of the temperature. (a) The solid black line shows the density of the fluid at coexistence (this study). The dashed line marks the  $T \rightarrow 0$  limit and the colored dots are literature data [42–44]. The red diamonds are densities computed with the interface-pinning method. (b) The solid black line shows the density of the solid at coexistence (this study), the dashed line is the  $T \rightarrow 0$  limit, and the colored dots represent literature data [42–44].

In the limit of large  $k$ ’s this converges to the trapezoidal rule of integration where forward and backward integrations yield the same result.

Which criterion to use in order to determine when the predictor-corrector iterations have converged? To answer this we note that since slopes are evaluated from finite  $NpT$  simulations, we expect a significant statistical error on the  $f$ ’s used above. If  $\bar{f}(t, y)$  is the theoretical slope,  $f(t, y) = \bar{f}(t, y) + e_f$  where  $e_f$  is drawn from a normal distribution with standard deviation  $\sigma_f$ . This error is estimated by dividing  $NpT$  simulations into statistically independent blocks [88]. The error on  $y_{i+1}^{k+1}$  is  $e_y = h e_f$  and  $\sigma_y = |h| \sigma_f$ . It is sensible to terminate the predictor-

corrector iteration when

$$|y_{i+1}^{k+1} - y_{i+1}^k| < \sigma_y \quad (28)$$

since this indicates that changes of  $y_{i+1}$ 's are mainly due to the statistical uncertainty on the slopes.

In summary, numerical integration of the Clausius-Clapeyron relation comes with errors from ignoring higher-order terms and from the statistical uncertainty of the slopes. To quantify the overall error of the integration we can compare to the accurate estimates from interface pinning at selected state points. As an example, for  $T_{48} = 2\varepsilon/k_B$  from the Clausius-Clapeyron integration we estimate the coexistence pressure to be  $31.7532\varepsilon/\sigma^3$ , which should be compared to  $31.8086(66)\varepsilon/\sigma^3$  for the interface-pinning method, see Table I. The error of the computed phase-transition line is not visible in most figures of this paper, with notable exceptions at low temperatures (error bars are shown in the below figures whenever errors are significant).

Figures 3 and 4 show coexistence pressures and densities, respectively, from this study and from the literature [42–44]. We note that the low-temperature estimates of Ref. 43 are not accurate, while the high-temperature estimates of Refs. 42–44 are consistent with our results. As a consistency check, we note that the computed coexistence line reaches the HS limit [89] when  $T \rightarrow 0$  (the dashed lines on Figs. 3 and 4 show the HS limits).

#### IV. COMPARING THE PREDICTIONS OF THE DIFFERENT HARD-SPHERE THEORIES

Having accurately located the WCA phase transition, we can now use this to test the four HS theories by comparing their predictions to the low-temperature WCA melting-line data.

##### A. Coexistence pressure and densities

Starting with the coexistence pressure, we first need coexistence information on the HS system. Fernandez et al. [90] estimate that the HS coexistence pressure is given by  $p_d = 11.5727(10)k_B T/d^3$ . This value is consistent with

$$p_d = 11.5712(10) k_B T/d^3 \quad (29)$$

computed more recently by Pieprzik et al. [89]; we use the latter value in this paper. In the zero-temperature limit, the HS diameter of the WCA interaction is  $d = r_c$ , which gives the coexistence pressure

$$p_\bullet = 8.1821(7) k_B T/\sigma^3. \quad (30)$$

The bullet subscript “ $\bullet$ ” refers throughout the paper to the HS limit of the WCA model that is approached when  $T \rightarrow 0$ , i.e., setting  $d = r_c$ .

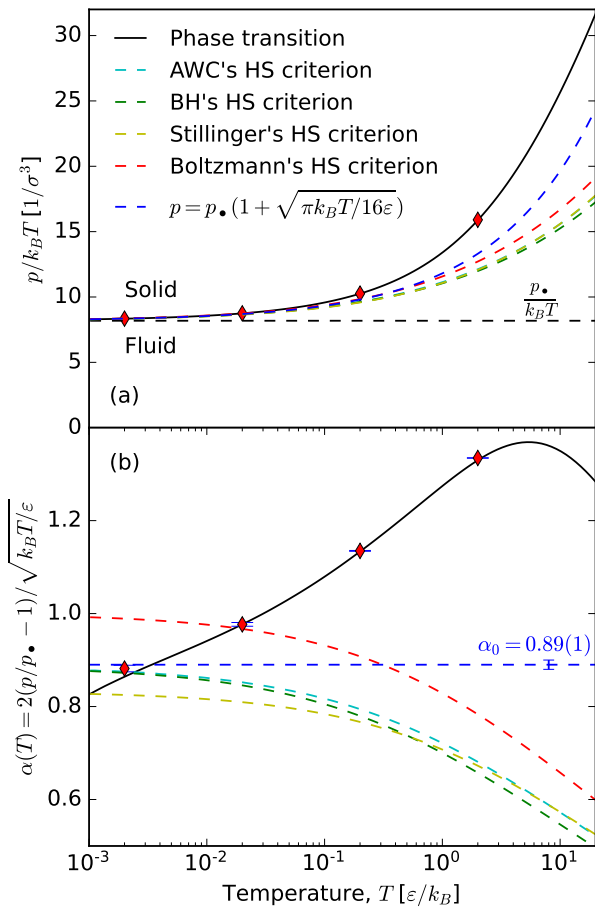


FIG. 5. Melting-line pressure compared to HS predictions. (a) The solid black line shows the reduced coexistence pressure,  $p/k_B T$ . The dashed lines show predictions of the HS theories (see text for details). The red diamonds show coexistence pressures computed with the interface-pinning method. (b)  $\alpha_p(T) = 2(p/p_\bullet - 1)/\sqrt{k_B T/\varepsilon}$  (Eq. (43)) along the computed phase transition line (black solid) and the theoretical predictions also shown in the upper panel (dashed lines). The blue dashed line ( $\alpha_0 = 0.89(1)$ ) is the  $T \rightarrow 0$  limit determined from coexistence densities, see Fig. 6(b). AWC and BH give accurate predictions in the low-temperature limit. The red diamonds are the results of the interface-pinning method where blue error bars indicate the statistical error. We note a systematic inaccuracy of the Clausius-Clapeyron integration (solid black) at the lowest temperatures.

The solid black line in Fig. 5(a) shows the coexistence pressure divided by the thermal energy,  $p/k_B T$ , and the black dashed line shows the  $d = r_c$  prediction. The predicted pressure is too low since the effective HS diameter is smaller than  $r_c$  at finite temperature where particles are allowed to overlap. In Fig. 5(a) we also consider other criteria for  $d$ 's (by insertions into Eq. (29)). At



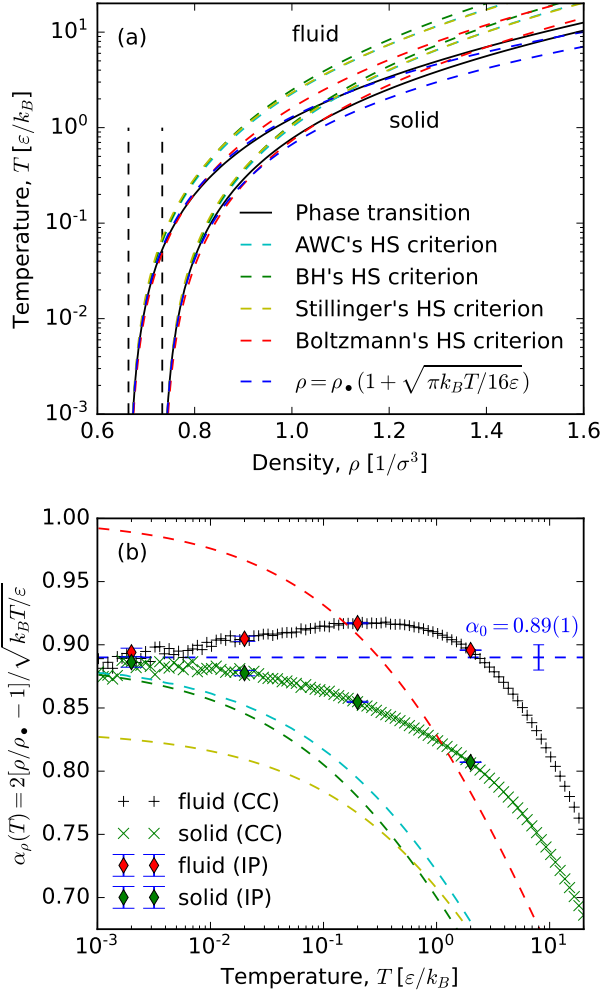


FIG. 6. Density-temperature phase diagram. (a) The solid black lines are the coexistence densities, compare Fig. 4. The vertical black dashed lines mark the  $T \rightarrow 0$  HS limits, i.e., the quantities  $\rho_\bullet^{(l)}$  and  $\rho_\bullet^{(s)}$ . The turquoise, green, yellow, and red dashed curves are predictions of the HS theories (see the text for details). The two blue dashed lines are the low-temperature fits  $\rho_l = \rho_\bullet^{(l)}[1 + 0.445\sqrt{k_B T/\varepsilon}]$  and  $\rho_s = \rho_\bullet^{(s)}[1 + 0.445\sqrt{k_B T/\varepsilon}]$ . (b) The black +’s show  $\alpha_\rho(T) = 2(\rho/\rho_\bullet - 1)/\sqrt{k_B T/\varepsilon}$  where the densities  $\rho$  and  $\rho_\bullet$  refer to the fluid. The green x’s is  $\alpha_\rho(T)$  using the solid densities. The red diamonds are densities computed with the interface-pinning method. The blue error bars indicate the 95% confidence interval. We find that the zero-temperature limit gives  $\alpha_0 = \lim_{T \rightarrow 0} \alpha(T) = 0.89(1)$ . The turquoise, green, yellow, and red dashed curves are predictions of the HS theories. The AWC and BH give the correct low-temperature limit within the statistical accuracy.

$T = 0.02\varepsilon/k_B$  the  $d = r_c$  criterion underestimates the coexistence pressure by 7%, while both the AWC and BH criterion give only a 1% error. Thus, the HS theories give a significant improvement of the predicted coexistence pressure. It is hard to decide from Fig. 5 which

theory is best since this depends on the temperature. We return below to the low-temperature limit that provides a definite answer. First, we turn to the HS theories’ predictions of the melting- and freezing densities.

Turning next to the freezing density, we first note that the HS fluid freezing density has been computed recently by Moir, Lue and Bannerman to the value [91]

$$\rho_d^{(l)} = 0.93890(7)/d^3 \quad (31)$$

and the melting density of the solid to

$$\rho_d^{(s)} = 1.03715(9)/d^3 \quad (32)$$

In the zero-temperature limit of the WCA system ( $d = r_c$ ) we get

$$\rho_\bullet^{(l)} = 0.66390(5)/\sigma^3 \quad (33)$$

and

$$\rho_\bullet^{(s)} = 0.73337(6)/\sigma^3 \quad (34)$$

When inserting the  $d$ ’s of the above HS criteria we get the temperature-dependent density predictions shown in Fig. 6(a) as colored dashed lines.

## B. Analytical treatment of the low-temperature limit

Inspired by the functional form of Stillinger’s and Boltzmann’s HS criteria (Eq. (20) and Eq. (12)) we write the low-temperature limit of the effective HS diameter as

$$d_\alpha = r_c \left(1 - \frac{\alpha_0}{6} \sqrt{k_B T/\varepsilon}\right) \text{ for } T \rightarrow 0, \quad (35)$$

which implies

$$d_\alpha^{-3} = r_c^{-3} \left(1 + \frac{\alpha_0}{2} \sqrt{k_B T/\varepsilon}\right) \text{ for } T \rightarrow 0. \quad (36)$$

For the Boltzmann criterion one has  $\alpha_0 = 1$  while Stillinger’s criterion gives  $\alpha_0 = \sqrt{\ln(2)} \simeq 0.83$ .

Since  $d$  is the same for the AWC and BH criteria in the  $T \rightarrow 0$  limit (see Sec. II B 3), the  $\alpha_0$ ’s are also identical. To evaluate  $\alpha_0$  we first note that the BH integral defining the HS diameter (Eq. (18)) can be written

$$d = r_c - \int_0^{r_c} \exp(-v(r)/k_B T) dr. \quad (37)$$

Since the WCA pair potential is purely repulsive, it reaches its minimum at zero when  $r = r_c$ . Thus at low temperatures the above integral is centered near  $r_c$ , i.e., near  $x = 0$  where  $x = r_c - r$ . Keeping the first non-vanishing term in a Taylor expansion we get

$$v(x) = \frac{1}{2} k_2 x^2 \text{ for } T \rightarrow 0 \quad (38)$$

TABLE II.  $\alpha_0$  values.

From simulations		0.89(1)
Boltzmann		1
AWC and BH	$\frac{1}{2}\sqrt{\pi} =$	0.886227...
Stillinger	$\sqrt{\ln(2)} =$	0.832555...

with (see Ref. 35)

$$k_2 \equiv \left. \frac{d^2 v}{dr^2} \right|_{r_c} = 36 \sqrt[3]{4\varepsilon/\sigma^2}. \quad (39)$$

Finding  $d$  from Eq. (37) involves solving a Gaussian integral in  $x$ . Expanding the upper limit of the integral to infinity, which is exact as  $T \rightarrow 0$ , we find

$$d = r_c - \sqrt{\frac{\pi k_B T}{2k_2}}. \quad (40)$$

By equating  $d = d_\alpha$  (Eqs. (40) and (35)) we get

$$\alpha_0 = \frac{6}{r_c} \sqrt{\frac{\pi\varepsilon}{2k_2}} \quad (41)$$

or  $\alpha_0 = \sqrt{\pi}/2 \cong 0.886227$ . The theoretical  $\alpha_0$  values are summarized in Table II.

To estimate  $\alpha_0$  from the simulations we insert  $d_\alpha^{-3}$  of Eq. (36) into Eq. (29) for the coexistence pressure, leading to

$$p = p_\bullet \left[ 1 + \frac{\alpha_0}{2} \sqrt{k_B T/\varepsilon} \right] \text{ for } T \rightarrow 0. \quad (42)$$

Thus, a way to determine  $\alpha_0$  is to define the function (Fig. 5(b))

$$\alpha_p(T) = \frac{2}{\sqrt{k_B T/\varepsilon}} \left[ \frac{p(T)}{p_\bullet} - 1 \right] \quad (43)$$

for which we note that  $\alpha_0 = \alpha(T)$  for  $T \rightarrow 0$ . Similarly, we get for the densities  $\rho = \rho_l$  or  $\rho = \rho_s$

$$\rho = \rho_\bullet \left( 1 + \frac{\alpha_0}{2} \sqrt{k_B T/\varepsilon} \right) \text{ for } T \rightarrow 0 \quad (44)$$

and define

$$\alpha_\rho(T) = \frac{2}{\sqrt{k_B T/\varepsilon}} \left[ \frac{\rho(T)}{\rho_\bullet} - 1 \right]. \quad (45)$$

Figure 6(a) shows the temperature dependence of the fluid and solid densities at coexistence (solid lines). These densities yield the  $\alpha_\rho(T)$ 's shown with black '+'s and green 'x's, respectively, on Fig. 6(b). From the low-temperature points we estimate  $\alpha_0 = 0.89(1)$ . The colored dashed lines show the predictions of the HS theories (the  $T \rightarrow 0$  limits agree with the values of Table II). We conclude that the AWC and BH theories gives excellent agreement as  $T \rightarrow 0$ . Figure 5(b) shows  $\alpha_p(T)$  computed using the coexistence pressure. In agreement with the

results for the  $\alpha_\rho(T)$ 's we find that  $\alpha_0 = 0.89(1)$  (blue dashed line).

The success of the AWC and BH theories suggests writing the coexistence pressure and densities as follows (inserting  $\alpha_0 = \sqrt{\pi}/2$  into Eqs. (42) and (44))

$$p = p_\bullet \left( 1 + \sqrt{\frac{\pi k_B T}{16\varepsilon}} \right) \quad (46)$$

and

$$\rho = \rho_\bullet \left( 1 + \sqrt{\frac{\pi k_B T}{16\varepsilon}} \right), \quad (47)$$

respectively, see the blue dashed lines of Figs. 3-6. Interestingly, this low-temperature approximation gives better predictions than the *neat* HS theories – even at high temperatures (with the exception of Boltzmann's criterion near  $T \simeq 0.5\varepsilon/k_B$ ). We do not have an explanation for this.

Equations (46) and (47) summarize an important result of this paper, providing an analytical HS approximation for the low-temperature freezing of the WCA fluid. This can be generalized to any other purely repulsive pair-potential that is truncated smoothly at  $r = r_c$  by the following steps:

1. Compute  $k_2$  using Eq. (39) and
2. derive  $\alpha_0$  within the BH theory by inserting  $k_2$  into Eq. (41).
3. Low-temperature predictions for coexistence pressure and densities are then provided by inserting  $\alpha_0$  into Eqs. (42) and (44), respectively.

## V. OUTLOOK

We have shown that HS theories give excellent predictions of the WCA melting line at low temperatures, in particular for the AWC and BH approximations. At higher temperatures the HS theories are less accurate. This is not surprising because the WCA model only resembles a HS system at low temperatures. How to predict the WCA melting-line pressures and coexistence densities at high temperatures? One possibility is to generalize the low-temperature HS approximation by considering the lines of constant excess entropy  $S_{\text{ex}}$  (this is the entropy in excess of the ideal gas entropy at the same density and temperature, a negative quantity that in some textbooks [92] is referred to as the residual entropy). For the HS system these lines are determined entirely by the density, i.e., they are vertical in the density-temperature phase diagram. In Ref. 35 it has been shown that the WCA system's structure and dynamics are near-invariant along the lines of constant excess entropy, which are referred to as isomorphs [93, 94]. An isomorph can be computed



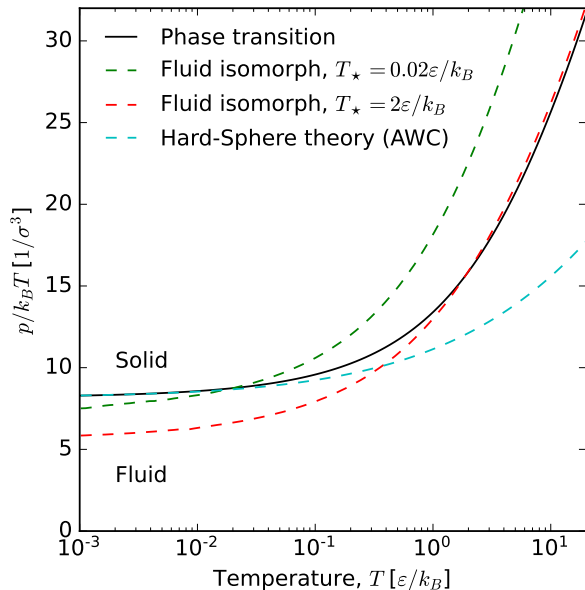


FIG. 7. The solid black line shows the reduced coexistence pressure  $p/k_B T$  as a function of the temperature. The red and green dashed curves are isomorphs of the fluid, i.e., lines along which the excess entropy,  $S_{ex}$ , is constant. The isomorphs touch the phase-transition line at  $T_* = 0.02\epsilon/k_B$  and  $T_* = 2\epsilon/k_B$ , respectively. The turquoise dashed line is the prediction of the AWC theory.

by numerical integration in the  $\ln T$ - $\ln \rho$  plane (e.g., using the fourth-order Runge-Kutta method (RK4) [35]) for which the required slope is  $f = 1/\gamma$  where [93, 95, 96]

$$\gamma \equiv \left( \frac{\partial \ln T}{\partial \ln \rho} \right)_{S_{ex}}. \quad (48)$$

The “density-scaling exponent”  $\gamma$  may be computed from virial- and potential-energy fluctuations in the  $NVT$  ensemble via the general statistical-mechanical identity

$\gamma = \langle \Delta W \Delta U \rangle / \langle (\Delta U)^2 \rangle$  [93]. Figure 7 shows the reduced pressure  $p/k_B T$  of two fluid isomorphs that overlap with the coexistence line at  $T_* = 0.02\epsilon/k_B$  and  $T_* = 2\epsilon/k_B$ , respectively (dashed green and red lines). For comparison, the turquoise dashed line shows the prediction of the reduced coexistence pressure of the AWC theory. For the entire temperature span the isomorphs gives predictions with an overall accuracy comparable to that of the best HS approximation (AWC).

Figures 8 and 9 show the structure and dynamics along the melting line and the fluid isomorph in reduced units [93]. Interestingly, the physics is more invariant along the coexistence lines than along the isomorph. This is in contrast to previous findings for the LJ system, where the opposite applies [97]. We note, however, that isomorphs only follow the coexistence lines to a first approximation. For the LJ system, accurate predictions for the thermodynamics of freezing and melting can be arrived at within the isomorph-theoretical perturbation framework proposed in Ref. 97 – we hope to apply the same method to the WCA system in the near future.

## ACKNOWLEDGMENT

This work was supported by the VILLUM Foundation’s Matter grant (No. 16515).

## AUTHOR DECLARATIONS

### Conflict of Interest

The authors have no conflicts to disclose.

## DATA AVAILABILITY

The data that support the findings of this study are openly available in Zenodo at <http://doi.org/10.5281/zenodo.6505218>, reference number 6505218.

[1] J.-P. Hansen and I. R. McDonald, *Theory of Simple Liquids: With Applications to Soft Matter*, 4th ed. (Academic, New York, 2013).  
[2] W. G. Hoover, S. G. Gray, and K. W. Johnson, “Thermodynamic properties of the fluid and solid phases for inverse power potentials,” *J. Chem. Phys.* **55**, 1128–1136 (1971).  
[3] W. G. Hoover, D. A. Young, and R. Grover, “Statistical mechanics of phase diagrams. i. inverse power potentials and the close-packed to body-packed cubic transition,” *J. Chem. Phys.* **56**, 2207–2210 (1972).  
[4] D. M. Heyes and A. C. Branka, “Physical properties of soft repulsive particle fluids,” *Phys. Chem. Chem. Phys.* **9**, 5570–5575 (2007).

[5] A. C. Branka and D. M. Heyes, “Pair correlation function of soft-sphere fluids,” *J. Chem. Phys.* **134**, 064115 (2011).  
[6] A. K. Bacher, T. B. Schröder, and J. C. Dyre, “The EXP pair-potential system. I. Fluid phase isotherms, isochores, and quasiuniversality,” *J. Chem. Phys.* **149**, 114501 (2019).  
[7] A. K. Bacher, T. B. Schröder, and J. C. Dyre, “The EXP pair-potential system. II. Fluid phase isomorphs,” *J. Chem. Phys.* **149**, 114502 (2018).  
[8] U. R. Pedersen, A. K. Bacher, T. B. Schröder, and J. C. Dyre, “The EXP pair-potential system. III. Thermodynamic phase diagram,” *J. Chem. Phys.* **150**, 174501 (2019).

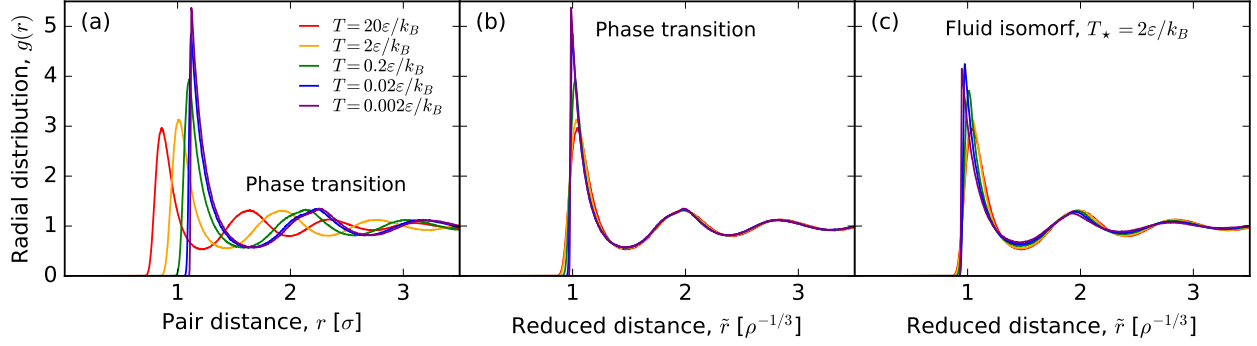


FIG. 8. (a) The radial distribution  $g(r)$  for the fluid at coexistence. (b) The radial distribution as a function of the reduced distance  $\tilde{r} = r\sqrt[3]{\rho}$  for the fluid at coexistence. (c) The radial distribution as a function of the reduced distance  $\tilde{r} = r\sqrt[3]{\rho}$  for a fluid isomorph that touch the coexistence line at  $T_* = 2\varepsilon/k_B$ .

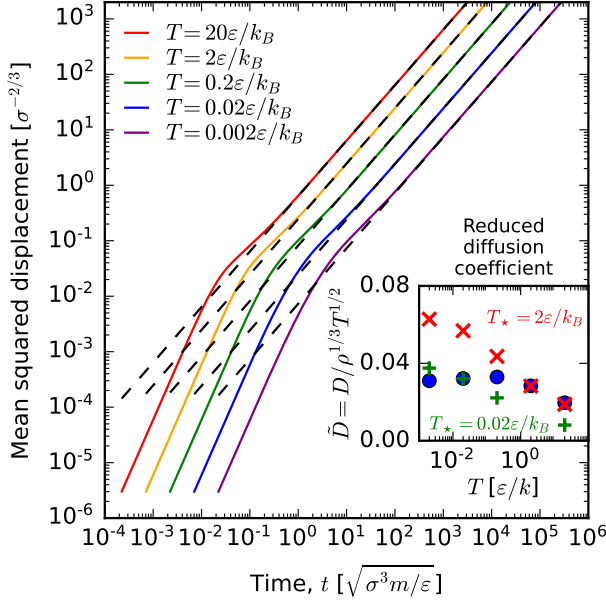


FIG. 9. The solid lines show the mean-square displacement  $\langle |\mathbf{r}(t) - \mathbf{r}(0)|^2 \rangle$  for selected state-points along the coexistence line (see Table I). The dashed lines are long-time fits to  $\langle |\mathbf{r}(t) - \mathbf{r}(0)|^2 \rangle = 6Dt$  where  $D$  is the diffusion coefficient. The dots in the inset show the reduced diffusion coefficient  $\tilde{D} = D\rho^{1/3}T^{1/2}$ . The red  $x$ 's and green  $+$ 's is the reduced diffusion coefficient for state points along the isomorphs with  $T_* = 2\varepsilon/k$  : B and  $T_* = 0.02\varepsilon/k_B$ , respectively.

[9] B. J. Alder and T. E. Wainwright, "Phase transition for a hard sphere system," *J. Chem. Phys.* **27**, 1208–1209 (1957).  
 [10] W. W. Wood and J. D. Jacobson, "Preliminary results from a recalculation of the Monte Carlo equation of state of hard spheres," *J. Chem. Phys.* **27**, 1207–1208 (1957).  
 [11] B. J. Alder and T. E. Wainwright, "Studies in molecular dynamics. I. general method," *J. Chem. Phys.* **31**, 459–466 (1959).

[12] B. J. Alder and T. E. Wainwright, "Studies in molecular dynamics. II. behavior of a small number of elastic spheres," *J. Chem. Phys.* **33**, 1439–1451 (1960).  
 [13] J. O. Hirschfelder, C. F. Curtiss, and R. B. Bird, *Molecular Theory of Gases and Liquids* (J. Wiley & Sons (New York), 1954).  
 [14] J. D. Bernal, "The Bakerian lecture, 1962. The structure of liquids," *Proc. R. Soc. London Ser. A* **280**, 299–322 (1964).  
 [15] B. Widom, "Intermolecular forces and the nature of the liquid state," *Science* **157**, 375–382 (1967).  
 [16] J. A. Barker and D. Henderson, "What is "liquid"? Understanding the states of matter," *Rev. Mod. Phys.* **48**, 587–671 (1976).  
 [17] J. D. Weeks, D. Chandler, and H. C. Andersen, "Role of repulsive forces in determining the equilibrium structure of simple liquids," *J. Chem. Phys.* **54**, 5237–5247 (1971).  
 [18] D. Chandler, J. D. Weeks, and H. C. Andersen, "Van der Waals picture of liquids, solids, and phase transformations," *Science* **220**, 787–794 (1983).  
 [19] F. C. Andrews, "A simple approach to the equilibrium statistical mechanics of two-dimensional fluids," *J. Chem. Phys.* **64**, 1941–1947 (1976).  
 [20] R. J. Speedy, F. X. Prielmeier, T. Vardag, E. W. Lang, and H.-D. Lüdemann, "Diffusion in simple fluids," *Molecular Physics* **66**, 577–590 (1989).  
 [21] D. Ben-Amotz and D. R. Herschbach, "Estimation of effective diameters for molecular fluids," *J. Phys. Chem.* **94**, 1038–1047 (1990).  
 [22] S. Hess, M. Kröger, and H. Voigt, "Thermomechanical properties of the WCA-Lennard-Jones model system in its fluid and solid states," *Physica A* **250**, 58–82 (1998).  
 [23] D. Ben-Amotz and G. Stell, "Hard sphere perturbation theory for fluids with soft-repulsive-core potentials," *J. Chem. Phys.* **120**, 4844–4851 (2004).  
 [24] D. Ben-Amotz and G. Stell, "Reformulation of weeks-chandler-andersen perturbation theory directly in terms of a hard-sphere reference system," *J. Phys. Chem. B* **108**, 6877–6882 (2004).  
 [25] D. M. Heyes and H. Okumura, "Equation of state and structural properties of the Weeks-Chandler-Andersen fluid," *J. Chem. Phys.* **124**, 164507 (2006).

- [26] L. Berthier and G. Tarjus, “Nonperturbative effect of attractive forces in viscous liquids,” *Phys. Rev. Lett.* **103** (2009), 10.1103/physrevlett.103.170601.
- [27] U. R. Pedersen, T. B. Schröder, and J. C. Dyre, “Repulsive reference potential reproducing the dynamics of a liquid with attractions,” *Phys. Rev. Lett.* **105** (2010), 10.1103/physrevlett.105.157801.
- [28] L. Berthier and G. Tarjus, “The role of attractive forces in viscous liquids,” *J. Chem. Phys.* **134**, 214503 (2011).
- [29] S. A. Khrapak, M. Chaudhuri, and G. E. Morfill, “Communication: Universality of the melting curves for a wide range of interaction potentials,” *J. Chem. Phys.* **134**, 241101 (2011).
- [30] L. Böhling, A. A. Veldhorst, T. S. Ingebrigtsen, N. P. Bailey, J. S. Hen, S. Toxvaerd, T. B. Schröder, and J. C. Dyre, “Do the repulsive and attractive pair forces play separate roles for the physics of liquids?” *J. Condens. Matter Phys.* **25**, 032101 (2012).
- [31] Z. E. Dell and K. S. Schweizer, “Microscopic theory for the role of attractive forces in the dynamics of supercooled liquids,” *Phys. Rev. Lett.* **115** (2015), 10.1103/physrevlett.115.205702.
- [32] L.-C. Valdès, J. Gerges, T. Mizuguchi, and F. Affouard, “Crystallization tendencies of modelled Lennard-Jones liquids with different attractions,” *J. Chem. Phys.* **148**, 014501 (2018).
- [33] J. Chattoraj and M. P. Ciamarra, “Role of attractive forces in the relaxation dynamics of supercooled liquids,” *Phys. Rev. Lett.* **124** (2020), 10.1103/physrevlett.124.028001.
- [34] Y. Zhou, B. Mei, and K. S. Schweizer, “Integral equation theory of thermodynamics, pair structure, and growing static length scale in metastable hard sphere and Weeks-Chandler-Andersen fluids,” *Phys. Rev. E* **101** (2020), 10.1103/physreve.101.042121.
- [35] E. Attia, J. C. Dyre, and U. R. Pedersen, “Extreme case of density scaling: The Weeks-Chandler-Andersen system at low temperatures,” *Phys. Rev. E* **103** (2021), 10.1103/physreve.103.062140.
- [36] S. S. Khali, D. Chakraborty, and D. Chaudhuri, “Two-step melting of the Weeks-Chandler-Andersen system in two dimensions,” *Soft Mat.* **17**, 3473–3485 (2021).
- [37] A. Banerjee and D. J. Wales, “Energy landscapes for a modified repulsive Weeks-Chandler-Andersen potential,” *J. Condens. Matter Phys.* **34**, 034004 (2021).
- [38] S. Toxvaerd, “Role of the attractive forces in a supercooled liquid,” *Phys. Rev. E* **103** (2021), 10.1103/physreve.103.022611.
- [39] A. Singh and Y. Singh, “How attractive and repulsive interactions affect structure ordering and dynamics of glass-forming liquids,” *Phys. Rev. E* **103** (2021), 10.1103/physreve.103.052105.
- [40] D. M. Heyes, S. Pieprzyk, and A. C. Brańka, “Application of cell models to the melting and sublimation lines of the Lennard-Jones and related potential systems,” *Phys. Rev. E* **104** (2021), 10.1103/physreve.104.044119.
- [41] Y. Zhou, B. Mei, and K. S. Schweizer, “Activated relaxation in supercooled monodisperse atomic and polymeric WCA fluids: Simulation and ECNLE theory,” *J. Chem. Phys.* **156**, 114901 (2022).
- [42] A. de Kuijper, J. A. Schouten, and J. P. J. Michels, “The melting line of the Weeks-Chandler-Anderson Lennard-Jones reference system,” *J. Chem. Phys.* **93**, 3515–3519 (1990).
- [43] A. Ahmed and R. J. Sadus, “Phase diagram of the Weeks-Chandler-Andersen potential from very low to high temperatures and pressures,” *Phys. Rev. E* **80** (2009), 10.1103/physreve.80.061101.
- [44] A. Mirzaeina, F. Feyzi, and S. Majid Hashemianzadeh, “Equation of state and Helmholtz free energy for the atomic system of the repulsive Lennard-Jones particles,” *J. Chem. Phys.* **147**, 214503 (2017).
- [45] J. E. Lennard-Jones, “On the determination of molecular fields. – I. from the variation of the viscosity of a gas with temperature,” *Proc. R. Soc. Lond. A* **106**, 441–462 (1924).
- [46] J. E. Lennard-Jones, “On the determination of molecular fields. – II. from the equation of state of a gas,” *Proc. R. Soc. Lond. A* **106**, 463–477 (1924).
- [47] N. Bailey, T. Ingebrigtsen, J. S. Hansen, A. Veldhorst, L. Böhling, C. Lemarchand, A. Olsen, A. Bacher, L. Costigliola, U. R. Pedersen, H. Larsen, J. C. Dyre, and T. Schröder, “RUMD: A general purpose molecular dynamics package optimized to utilize GPU hardware down to a few thousand particles,” *SciPost Phys.* **3** (2017), 10.21468/scipostphys.3.6.038.
- [48] D. Frenkel and B. Smit, *Understanding molecular simulation: from algorithms to applications*, 2nd ed. (Academic Press, San Diego, 2002).
- [49] N. Grønbech-Jensen, “Complete set of stochastic Verlet-type thermostats for correct Langevin simulations,” *Mol. Phys.* **118**, e1662506 (2019).
- [50] N. Grønbech-Jensen and O. Farago, “Constant pressure and temperature discrete-time Langevin molecular dynamics,” *J. Chem. Phys.* **141**, 194108 (2014).
- [51] N. Grønbech-Jensen, N. R. Hayre, and O. Farago, “Application of the G-JF discrete-time thermostat for fast and accurate molecular simulations,” *Comput. Phys. Commun.* **185**, 524–527 (2014).
- [52] D. M. Heyes and H. Okumura, “Equation of state and structural properties of the Weeks-Chandler-Andersen fluid,” *J. Chem. Phys.* **124**, 164507 (2006).
- [53] R. W. Zwanzig, “High-temperature equation of state by a perturbation method. i. nonpolar gases,” *J. Chem. Phys.* **22**, 1420–1426 (1954).
- [54] J. S. Rowlinson, “An equation of state of gases at high temperatures and densities,” *Mol. Phys.* **7**, 349–361 (1964).
- [55] H. L. Frisch, J. L. Katz, E. Praestgaard, and J. L. Lebowitz, “High-temperature equation of state – argon,” *J. Phys. Chem.* **70**, 2016–2020 (1966).
- [56] J. A. Barker and D. Henderson, “Perturbation theory and equation of state for fluids. II. a successful theory of liquids,” *J. Chem. Phys.* **47**, 4714–4721 (1967).
- [57] H. C. Andersen, J. D. Weeks, and D. Chandler, “Relationship between the hard-sphere fluid and fluids with realistic repulsive forces,” *Phys. Rev. A* **4**, 1597–1607 (1971).
- [58] L. Verlet and J.-J. Weis, “Perturbation theory for the thermodynamic properties of simple liquids,” *Mol. Phys.* **24**, 1013–1024 (1972).
- [59] F. Lado, “Choosing the reference system for liquid state perturbation theory,” *Mol. Phys.* **52**, 871–876 (1984).
- [60] G. Kahl, “Analytic representation for the pair-correlation function of a hard-sphere Yukawa system,” *Mol. Phys.* **67**, 879–889 (1989).
- [61] J. Chang and S. I. Sandler, “A real function representation for the structure of the hard-sphere fluid,” *Mol.*

- Phys. **81**, 735–744 (1994).
- [62] A. Trokhymchuk, I. Nezbeda, J. Jirsák, and D. Henderson, “Hard-sphere radial distribution function again,” *J. Chem. Phys.* **123**, 024501 (2005).
  - [63] D. Henderson, “Analytic methods for the Percus-Yevick hard sphere correlation functions,” *Condens. Matter Phys.* **12**, 127–135 (2009).
  - [64] J. C. Dyre, “Simple liquids’ quasiuniversality and the hard-sphere paradigm,” *J. Phys. Condens. Matter* **28**, 323001 (2016).
  - [65] J. R. Solana, *Perturbation theories for the thermodynamic properties of fluids and solids* (CRC Press, London, England, 2019).
  - [66] B. P. Akhouri and J. R. Solana, “On the choice of the effective diameter in the high-temperature expansion for the Lennard-Jones fluid,” *Mol. Phys.* (2022), 10.1080/00268976.2022.2028918.
  - [67] T. van Westen, M. Hammer, B. Hafskjold, A. Aasen, J. Gross, and Ø. Wilhelmsen, “Perturbation theories for fluids with short-ranged attractive forces: A case study of the Lennard-Jones spline fluid,” *J. Chem. Phys.* **156**, 104504 (2022).
  - [68] L. Boltzmann, *Lectures on Gas Theory* (Dover Publications, 1864).
  - [69] M. S. Wertheim, “Exact solution of the Percus-Yevick integral equation for hard spheres,” *Phys. Rev. Lett.* **10**, 321–323 (1963).
  - [70] W. R. Smith, D. J. Henderson, P. J. Leonard, J. A. Barker, and E. W. Grundke, “Fortran codes for the correlation functions of hard sphere fluids,” *Mol. Phys.* **106**, 3–7 (2008).
  - [71] P. Virtanen et al., “SciPy 1.0: Fundamental Algorithms for Scientific Computing in Python,” *Nat. Methods* **17**, 261–272 (2020).
  - [72] R. Piessens, E. De Doncker-Kapenga, C. Uberhuber, and D. K. Kahaner, *Quadpack*, Springer series in computational mathematics (Springer, Berlin, Germany, 1983).
  - [73] F. H. Stillinger, “Phase transitions in the gaussian core system,” *J. Chem. Phys.* **65**, 3968–3974 (1976).
  - [74] C. N. Likos, “Effective interactions in soft condensed matter physics,” *Phys. Rep.* **348**, 267–439 (2001).
  - [75] U. R. Pedersen, “Direct calculation of the solid-liquid Gibbs free energy difference in a single equilibrium simulation,” *J. Chem. Phys.* **139**, 104102 (2013).
  - [76] U. R. Pedersen, F. Hummel, G. Kresse, G. Kahl, and C. Dellago, “Computing Gibbs free energy differences by interface pinning,” *Phys. Rev. B* **88** (2013), 10.1103/physrevb.88.094101.
  - [77] V. Thapar and F. A. Escobedo, “Extensions of the interfacial pinning method and application to hard core systems,” *J. Chem. Phys.* **141**, 124117 (2014).
  - [78] U. R. Pedersen, F. Hummel, and C. Dellago, “Computing the crystal growth rate by the interface pinning method,” *J. Chem. Phys.* **142**, 044104 (2015).
  - [79] B. Cheng, E. A. Engel, J. B., C. Dellago, and M. Ceriotti, “Ab initio thermodynamics of liquid and solid water,” *PNAS* **116**, 1110–1115 (2019).
  - [80] R. S. Newman, S. N., J. Dshemuchadse, and S. C. Glotzer, “Shape-controlled crystallisation pathways in dense fluids of ccp-forming hard polyhedra,” *Mol. Phys.* **117**, 3819–3826 (2019).
  - [81] K. G. Steenbergen, E. Pahl, and P. Schwerdtfeger, “Accurate, large-scale density functional melting of Hg: Relativistic effects decrease melting temperature by 160 K,” *J. Phys. Chem. Lett.* **8**, 1407–1412 (2017).
  - [82] A. K. Sharma and F. A. Escobedo, “Nucleus-size pinning for determination of nucleation free-energy barriers and nucleus geometry,” *J. Chem. Phys.* **148**, 184104 (2018).
  - [83] Y. Zou, S. Xiang, and C. Dai, “Investigation on the efficiency and accuracy of methods for calculating melting temperature by molecular dynamics simulation,” *Comput. Mater. Sci.* **171**, 109156 (2020).
  - [84] L. Zhu, J. Janssen, S. Ishibashi, F. Körmann, B. Grabowski, and J. Neugebauer, “A fully automated approach to calculate the melting temperature of elemental crystals,” *Comput. Mater. Sci.* **187**, 110065 (2021).
  - [85] W. Lechner and C. Dellago, “Accurate determination of crystal structures based on averaged local bond order parameters,” *J. Chem. Phys.* **129**, 114707 (2008).
  - [86] D. A. Kofke, “Gibbs-Duhem integration: a new method for direct evaluation of phase coexistence by molecular simulation,” *Mol. Phys.* **78**, 1331–1336 (1993).
  - [87] D. A. Kofke, “Direct evaluation of phase coexistence by molecular simulation via integration along the saturation line,” *J. Chem. Phys.* **98**, 4149–4162 (1993).
  - [88] H. Flyvbjerg and H. G. Petersen, “Error estimates on averages of correlated data,” *J. Chem. Phys.* **91**, 461–466 (1989).
  - [89] S. Pieprzyk, M. N. Bannerman, A. C. Brańka, M. Chudak, and D. M. Heyes, “Thermodynamic and dynamical properties of the hard sphere system revisited by molecular dynamics simulation,” *Phys. Chem. Chem. Phys.* **21**, 6886–6899 (2019).
  - [90] L. A. Fernandez, V. Martin-Mayor, B. Seoane, and P. Verrocchio, “Equilibrium fluid-solid coexistence of hard spheres,” *Phys. Rev. Lett.* **108** (2012), 10.1103/physrevlett.108.165701.
  - [91] C. Moir, L. Lue, and M. N. Bannerman, “Tethered-particle model: The calculation of free energies for hard-sphere systems,” *J. Chem. Phys.* **155**, 064504 (2021).
  - [92] I. Prigogine and R. Defay, *Chemical thermodynamics* (Prentice Hall Press, 1954).
  - [93] N. Gnan, T. B. Schröder, U. R. Pedersen, N. P. Bailey, and J. C. Dyre, “Pressure-energy correlations in liquids. IV. ‘Isomorphs’ in liquid phase diagrams,” *J. Chem. Phys.* **131**, 234504 (2009).
  - [94] T. B. Schröder and J. C. Dyre, “Simplicity of condensed matter at its core: Generic definition of a Roskilde-simple system,” *J. Chem. Phys.* **141**, 204502 (2014).
  - [95] J. C. Dyre, “Hidden scale invariance in condensed matter,” *J. Phys. Chem. B* **118**, 10007–10024 (2014).
  - [96] J. C. Dyre, “Perspective: Excess-entropy scaling,” *J. Chem. Phys.* **149**, 210901 (2018).
  - [97] U. R. Pedersen, L. Costigliola, N. P. Bailey, T. B. Schröder, and J. C. Dyre, “Thermodynamics of freezing and melting,” *Nat. Commun.* **7** (2016), 10.1038/ncomms12386.